UNIVERSIDAD DE CHILE
FACULTAD DE CIENCIAS FÍSICAS Y MATEMÁTICAS
DEPARTAMENTO DE INGENIERÍA CIVIL

SIMULATION OF THE SEISMIC RESPONSE OF THE SANTIAGO BASIN, CHILE

TESIS PARA OPTAR AL GRADO DE MAGÍSTER EN CIENCIAS DE LA INGENIERIA,
MENCIÓN INGENIERÍA ESTRUCTURAL, SÍSMICA Y GEOTÉCNICA

MEMORIA PARA OPTAR AL TÍTULO DE INGENIERO CIVIL

JOSÉ IGNACIO BUSTOS FONSECA

PROFESOR GUÍA:

CÉSAR PASTÉN PUCHI

MIEMBROS DE LA COMISIÓN:

SERGIO RUIZ TAPIA

RODRIGO ASTROZA EULUFI

SANTIAGO DE CHILE
2021

RESUMEN DE LA TESIS PARA OPTAR AL GRADO DE MAGISTER EN CIENCIAS DE LA INGENIERÍA, MENCIÓN INGENIERÍA ESTRUCTURAL, SÍSMICA Y GEOTÉCNICA Y AL TÍTULO DE INGENIERO CIVIL
POR: JOSÉ IGNACIO BUSTOIS FONSECA
FECHA: ALGUN DIA
PROFESOR GUÍA: CÉSAR PASTÉN PUCHI

SIMULATION OF THE SEISMIC RESPONSE OF THE SANTIAGO BASIN, CHILE

Two mega-thrust earthquakes have struck the Santiago city, the economic and political center of Chile with more than 5.5 million inhabitants, causing extensive damage and high seismic intensities. In this study, we use the results of an ambient seismic noise tomography, gravimetric studies, deep wells, and local geophysical methods to develop three representative cross-sections along the Santiago Basin. Then we perform 2D dynamic numerical simulations using the finite-difference code 2DFD_DVS. The input ground motions are impulse signals polarized in the longitudinal, transverse, and vertical directions with respect to the profiles imposed inside the model domain. In addition, the one-dimensional (1D) response of the model was calculated to compare with the two-dimensional (2D) response. The constitutive model of the materials is a generalized Maxwell body with a constant quality factor. The velocity time-histories obtained in the model surface highlight significant amplification of the softer sediments in the basin and longer strong ground motion due to surface waves generated at the boundaries of rock outcrops. Aggravation factors of the 2D model with respect to the 1D response are calculated and indicate that the 1D approach resembles the 2D response in sites with stiff soils, but it cannot capture the basin edge effects in sites with soft sediments. Records of the six seismic stations closest to CD and EW cross-sections for the 2015 Mw 8.4 Illapel megathrust earthquake are consistent with numerical simulations in the frequency domain.

RESUMEN DE LA TESIS PARA OPTAR AL GRADO DE MAGISTER EN CIENCIAS DE LA INGENIERÍA, MENCIÓN INGENIERÍA ESTRUCTURAL, SÍSMICA Y GEOTÉCNICA Y AL TÍTULO DE INGENIERO CIVIL
POR: JOSÉ IGNACIO BUSTOIS FONSECA
FECHA: ALGUN DIA
PROFESOR GUÍA: CÉSAR PASTÉN PUCHI

SIMULATION OF THE SEISMIC RESPONSE OF THE SANTIAGO BASIN, CHILE

Dos mega terremotos han afectado la ciudad de Santiago en las últimas décadas, el centro económico y político de Chile con más de 5.5 millones de habitantes, causando altas intensidades sísmicas y cuantiosos daños. En este estudio, utilizamos los resultados de una tomografía de ruido sísmico ambiental, estudios gravimétricos, pozos profundos y métodos geofísicos locales para desarrollar y analizar modelos numéricos de tres secciones transversales representativas de la geomorfología de la Cuenca de Santiago. Las simulaciones numéricas dinámicas bidimensionales (2D) se realizaron utilizando el código de diferencias finitas 2DFD_DVS. La fuente sísmica en el modelo corresponde a un pulso de Gabor polarizado en las direcciones longitudinal, transversal y vertical de cada sección transversal. Además, se calculó la respuesta unidimensional (1D) de los modelos para compararla con la respuesta 2D. El modelo constitutivo de los materiales es un cuerpo Maxwell generalizado con un factor de calidad constante. Los sismogramas sintéticos obtenidos en la superficie del modelo muestran una amplificación significativa de los sedimentos más blandos de la cuenca y duraciones del movimiento fuerte más extensas debido a las ondas superficiales generadas en los bordes de los afloramientos de roca. Se calcularon factores de agravamiento de amplificación sísmica del modelo 2D con respecto a la respuesta 1D, los cuales indican que el enfoque 1D se asemeja a la respuesta 2D en sitios con suelos rígidos, pero que la aproximación 1D no captura los efectos de borde de la cuenca en sitios con presencia de sedimentos blandos. Las simulaciones y patrones de amplificación son consistentes con registros reales del terremoto de Illapel 2015 de Mw 8.3 medidos en seis estaciones sísmicas cercanas a las secciones transversales estudiadas.

.

Agradecimientos

Quiero primero que todo agradecer a mis padres, Jacqueline y Marco y a mi hermana, Cote, por todo el apoyo y amor que me han dado a lo largo de toda mi vida, especialmente por haberme dado esta oportunidad única de estudiar y por estar siempre preocupados de darme lo necesario y más. Gracias a los tres por siempre inculcarme el estudio y empujarme para ser cada día mejor persona.

A mi familia, gracias por todas las enseñanzas, por siempre estar ahí, por incentivarme a seguir adelante y por sobre todo gracias por esas juntas familiares que siempre me han llenado de tanta energía para comenzar las semanas. Quiero agradecer a mi abuela Margarita por el amor entregado y espero que esto te llene de orgullo, quiero aprovechar de agradecer a mis abuelos, Carmen, Óscar y Moisés, con quienes me hubiese encantado compartir este importante logro personal.

A mi primo, Rodrigo, por llevarme contigo a tu trabajo cuando yo era pequeño e indirectamente hacer que me apasionara por el mundo de la construcción, lo que me generó un objetivo que finalmente me llevó donde estoy ahora.

A Catalina, mi pareja, mejor amiga y compañera de vida, gracias por tu apoyo incondicional sin duda fuiste un pilar fundamental a lo largo de esta etapa y sé que lo seguirás siendo a lo largo de mi vida, acompañándome siempre en los momentos buenos, pero más aún en los momentos difíciles, gracias por tu amor incondicional y por creer en mi incluso más de lo que yo lo hago.

A mi familia Malhue Vidal y compañía, por el apoyo y enorme cariño que me han entregado en todo momento, son una familia increíble de la que he aprendido muchísimo, gracias por ser parte de mi vida.

Quiero agradecer a mis chorokis por todas esas aventuras locas que hemos compartido juntos y por todas las que vendrán, gracias por contagiarme con su alegría y estar siempre presente a pesar de que todos hemos tomado caminos diferentes.

A mis amigos de la U, gracias por la buena onda y por siempre compartir sus conocimientos, sin duda me llevo lo mejor de cada uno. En especial quiero agradecer a Nicolás C. por todas esas horas de trabajo, y por indirectamente empujarme a sacar lo mejor de mí. A Belén, gracias por la buena onda y por siempre acordarme de las cosas importantes. También quiero agradecer a Tania A. por aguantarme por tanto tiempo y por siempre ser tan motivada, espero te vaya increíble, aunque sé que llegaras lejos porque eres mucho más crack de lo que crees.

Finalmente quiero agradecer a mi profesor guía, César Pastén, gracias por su constante apoyo a lo largo de todo el desarrollo de este trabajo, por todo el conocimiento entregado y por esas innumerables reuniones muy agradables en las que intenté siempre absorber todas sus enseñanzas y consejos, de verdad muchas gracias y espero poder seguir aprendiendo de usted.

Al Fondo Nacional de Desarrollo Científico y Tecnológico (FONDECYT) por financiar este trabajo mediante el proyecto 1190995. Esta tesis fue parcialmente apoyada por la infraestructura de supercómputo del NLHPC (ECM-02).

Contents

List of Tables

List of Figures

Chapter 1 :

Introduction

1.1 Introduction

In the last decades, two major earthquakes have affected the Santiago Basin, the 1985 Mw 8.0 Valparaiso and the 2010 Mw 8.8 Maule earthquakes. In these events, MSK macro seismic-intensities varying between VI-VIII along the basin were reported, and this variation has been attributed to the characteristics of the surface geology of the basin (Leyton et al., 2011; Astroza et al., 2012), revealing the existence of areas where site effects, such as amplification and increased duration of ground motion, are generated.

The Santiago Basin has been studied by several authors with the aim of identifying and explaining the factors that directly affect the phenomenon of seismic amplification. Araneda et al. (2000), Yañez et al. (2015), and González et. al. (2018) developed gravimetric studies along the basin showing irregular morphology with relatively shallow sediments with three main depocenters reaching maximum depths of approximately 600 m. The results of these studies are relatively similar, and the main differences are due to the spatial distribution of the dataset they adopted. Pastén (2007) and Bonnefoy-Claudet et al. (2009) estimated the predominant frequencies in softer deposits mainly located in the northeastern part of the basin and were unable to identify a predominant frequency in stiffer soils, such as gravel and alluvial soils, because horizontal-to-vertical spectral ratios (HVSRs) tend to be flat with amplitudes lower than 2.0. Pilz et al. (2010) proposed a shear wave velocity (Vs) model with a single soil type for the central area of the Santiago Basin. The dimensions of their model are 26 km × 12 km to a depth of 600 m, i.e., a reduced area of the basin. Leyton et al. (2011) described the surface geology of the basin and proposed a seismic zonation which considers two areas based on the dynamic properties of shallower soils, predominant vibrations frequencies, as well as macro seismic-intensities reported during the 1985 Mw 8.0 Valparaiso earthquake. Pastén et al. (2016) calculated cross-correlations of the vertical component of ambient seismic noise in the frequency domain between seismic station pairs to estimate phase velocity dispersion curves between 0.1 and 8.0 Hz, obtaining deep shear wave velocity profiles down to 5 km depth. Salomón et al. (2021) determined a three-dimensional (3D) model of shear wave velocity for the bedrock of the Abanico Formation underlying the Santiago city metropolitan area valid from 0.6 to 5 km depth using ambient seismic noise tomography.

1.2 General objective

Generate three representative cross-sections of the Santiago Basin, defining the geomorphology and the dynamic properties of sediments and bedrock to perform 1D and 2D numerical simulations inducing plane wavefronts from the base of the basin to make comparisons between 1D and 2D dynamic response to identify areas where

site effects occur and then compare the synthetic response generated for 2D models with seismic evidence.

1.3 Specific objectives

The specific objectives consist in:

- Collect information from several studies and generate three representative cross-sections of the basin in different directions (EW, NS, and CD cross-sections in Fig. 1), define the geomorphology and the dynamic properties of sediments and bedrock, based on shear wave velocity profiles obtained from environmental noise measurements and the seismic noise tomography of Salomon et al. (2020).
- Perform 1D and 2D numerical simulations inducing plane wavefronts from the base of the basin using the finite-difference code 2DFD_DVS (Moczo and Kristek 2007) to make comparisons between 1D and 2D dynamic response of each cross-section considering the superficial synthetic records, H/V spectral ratios, as well as amplification and aggravation factors along the surface of the models to identify areas where site effects occur and analyze the limitations of 1D simulations.
- Compare the synthetic response generated for 2D models with the seismic evidence available for the 2015 Mw 8.4 Illapel megathrust earthquake thanks to the CSN's accelerograph's network (National Seismological Center).

1.4 Structure of the work

This thesis consists of 6 chapters beginning with an introduction of the study in Chapter 1, then Chapter 2 describes the geological and Seismotectonic framework of the Santiago basin detailing quaternary sediments and the observations during the last earthquakes that have affected it. Chapter 3 describes the process of constructing the cross sections studied together with the description of the simulations performed in each cross section. Chapter 4 shows the results obtained from 2D simulations and analyses and comparisons are performed between the 1D and 2D response. Chapter 5 shows seismic evidence of amplification for the Illapel earthquake and compares it to the numerical simulations performed. Finally, chapter 6 gives a discussion of the work and the main conclusions.

Chapter 2 :

Geologic and Seismotectonic Framework

2.1 Geologic and Seismotectonic Framework

Santiago is located in middle of Central Chile region, where the seismotectonic is strongly controlled by the subduction of the oceanic Nazca plate underneath the continental South American plate, with a convergence rate of approximately 66 mm/year (Vigny et al., 2009) and producing frequently large magnitude earthquakes (Ruiz and Madariaga, 2018). The city of Santiago (Fig. 1) was founded in a sedimentary basin located in the central zone of continental Chile, and it has an extension of 90 km in the north-south direction and 40 km in the east-west direction. Gravimetric studies showed that the Santiago basin is relatively shallow and has an irregular geometry presenting three main depocenters that reach approximately 600 m depth (Araneda et al., 2000; Gonzalez et al., 2018). Leyton et al. (2011) described the surface geology of the Santiago basin based on the granulometric features of the first 30 m, defining eight units of soil along the basin. The north of the basin present deposits of silt and clay with gravel, sand, and ash interbeds. These soils are mainly soft, generating large impedance with the bedrock (unit VII, Fig. 1). Towards the west, the basin is composed of shallow pyroclastic deposits of over 20 m thick known as Pudahuel Ignimbrite, with sand, silt, and gravel interbeds (unit VI, Fig. 1). These deposits merge with the northern fine-grained soils. The basin's central part was filled by the coalescence of the Mapocho and Maipo rivers with coarse-grained sediments, dominantly sandy gravels of medium to high density, known as the Santiago gravel (unit II, Fig. 1), that has both high strength and stiffness. To the east, the basin has deposits that correspond to small alluvial fans located at the slope toe of the Andes mountains. These sediments are moderately rigid and are mainly composed of blocks and subangular gravel in sandy-clayey matrix, interleaved by sand, silt, and clay.

Monge & Astroza (1989), Leyton etal. (2010), and Vergara & Verdugo (2015) pointed out that the most serious structural damage during the 1985 Mw 8.0 Valparaiso and the 2010 Mw 8.8 Maule earthquakes occurred in the northwestern part of the basin, an area predominantly composed of soft soils, thus, pointing out that surface geology had a strong influence on the seismic response of the Santiago basin. Proof of this was that MSK-64 macro-seismic intensities above 7.5 were reported in limos, clays and ignimbrite deposits, while in gravel deposits macro-seismic intensities lower than 6.0 were reported. The high intensities recorded in the soft soils of the northwest are directly related to the low values of shear wave velocities and the high depths of these deposits, which result in low predominant frequencies. All these effects were also evidenced for the 2010 Mw 8.8 Maule earthquake, confirming the effect of surface geology on the dynamic response of the Santiago basin.

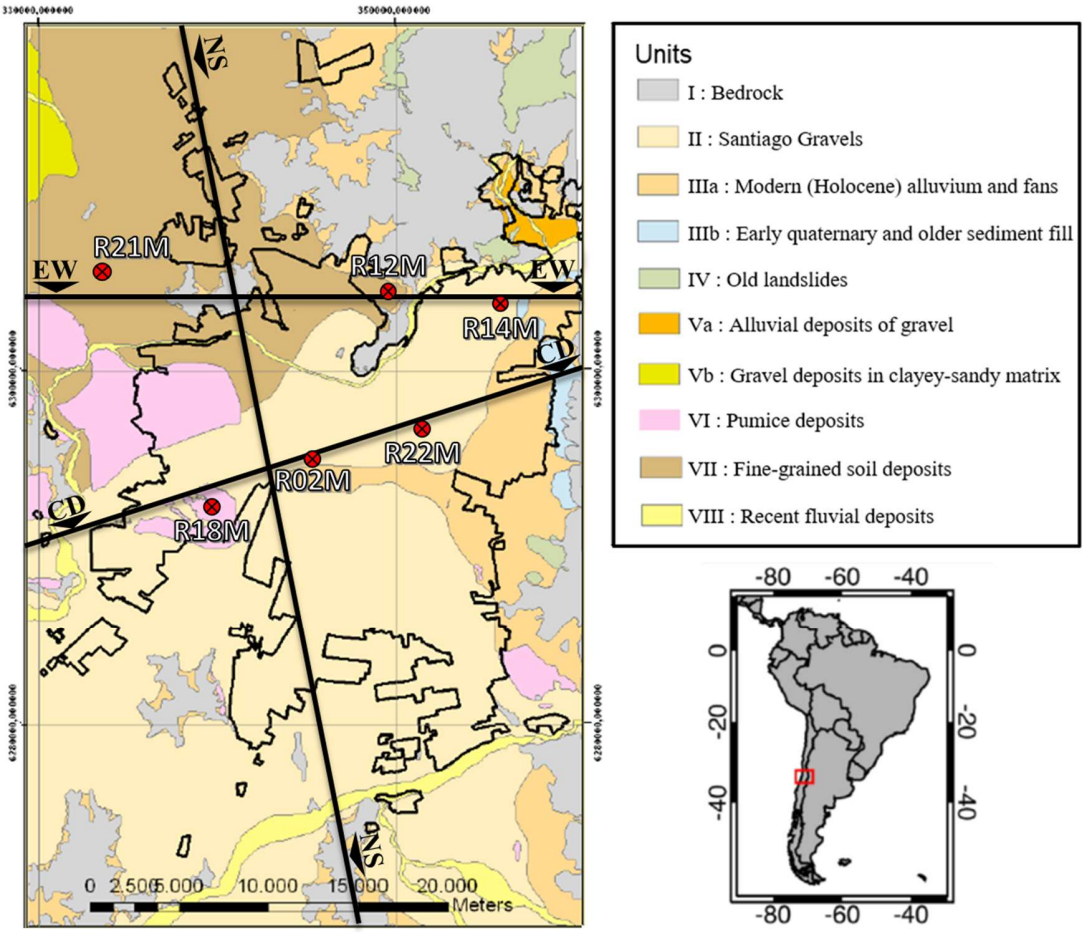

Figure 1 Surface geology of the Santiago basin proposed by Leyton et al. (2010). the areas bounded by the black lines represent the urban areas of Santiago.

Chapter 3

Numerical Models

3.1 Geological Cross-sections

In this study, we analyzed three cross-sections along the Santiago Basin, one in the east west direction (EW in Fig. 1), another in the North south direction (NS in Fig. 1), and the last one in the northeast direction (CD in Fig. 1). To determine the geology of the cross-sections, we use wells with more than 200 m depth obtained from General Water Directorate (GWD) and studies developed by Wall et al. (1999), Milovic (2000), Fernández (2001, 2003), Sellés & Gana (2001), Rauld (2002) and Fock (2005). From these wells, geotechnical profiles were generated in which the most massive strata are considered, and thin layers of other soil types were ignored. For all cases where the wells did not reach the bedrock, we assumed that the soil found at the maximum well depth extends to the interface with the bedrock inferred from the gravimetric studies. To build the 2D geological cross-sections, we considered the information of wells located along each cross-section, as well as the location of the bedrock based on the available gravimetric studies (Araneda et al. 2000; Gonzalez et al. 2018). We also considered the superficial geology reported in Leyton et al. (2011) for the shallower soil layers. For the northern part of Santiago Basin, we used information from the 2D geological cross-sections proposed by Galvez (2012). The three defined cross-sections are shown in Fig 3.

3.2 Dynamic properties

To estimate the shear wave velocity of the soils, we use measurements of ambient seismic noise reported by Pasten (2007), and we complement them with measurements in areas where scarce or no information was available. A total of 24 sites were measured, mainly concentrated in the northeastern part of the basin. The aim was to generate a robust model for softer soils, which have the greatest effects on seismic amplification according to Leyton et al. (2011) and Monge & Astroza (1989).

In the new measurement campaigns, we recorded 40 minutes of ambient seismic noise on each site using four 3G Trominos (Triaxial sensor with a natural frequency of ~5 Hz). The spatial distribution of the sensors depended on the spatial limitations of each site, allowing the use of rectangular or linear arrangements, with a maximum instrumental distance between 20 to 200 m. Using all the data, we conduct cross-correlations between measured records following the methodology proposed by Pasten et al. (2016), based on the study of Ekström et al. (2009), to obtain a representative phase velocity dispersion curve. We also calculated single station Rayleigh wave ellipticity with the RayDec software developed by Hobiger (2009) and determined predominant frequencies using the HVSR method. With this information, we performed a two-step joint inversion following the methodology developed in Hobiger et al. (2013) using the Dinver subroutine of the Geopsy software developed by Wathelet (2008). The first step of the inversion considers adjusting the dispersion

curve with velocity profiles searched in a wide range of shear wave velocities of soils and layer thickness ranges that depend primarily on the minimum wavelengths obtained from the dispersion curves. The second step consists of a joint inversion that considers the dispersion curve, the ellipticity curve, and predominant frequency of the site. The joint inversion narrows the search range of Vs based on the results obtained in the first step. This methodology allows obtaining deeper shear wave velocity profiles with a good fit to the target input curves.

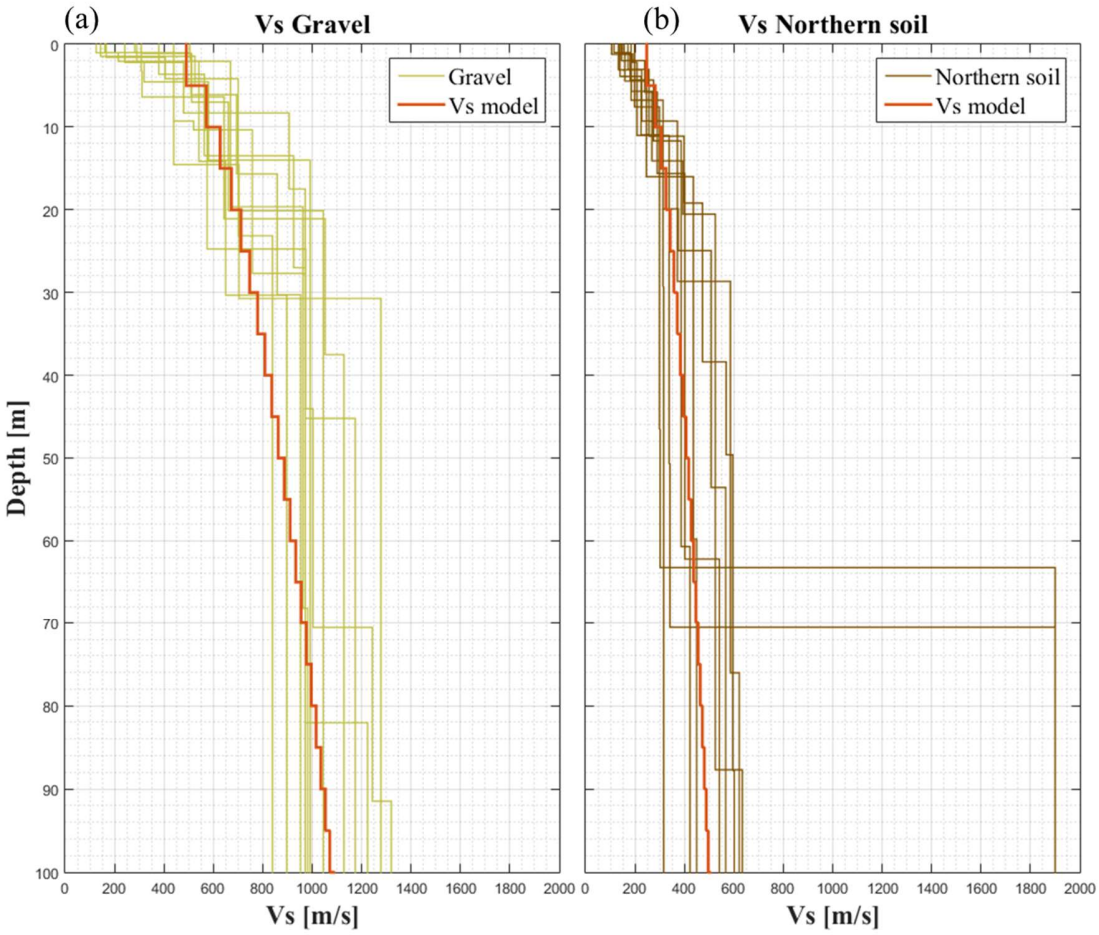

Figure 2 Vs profiles up to a depth of 100 m, in orange highlights the Vs model used for simulations. (a) shows the Santiago's gravel, and (b) shows the fine soils of the north.

Fig.2 shows the variation of Vs with depth for gravels and the northern fine soils (shown as Unit VII in Fig 1 and Silty Clay in Fig. 3). We defined a transition zone in the NS cross-section (Clayey gravel, clay, and gravel, sandy clay, clayey sand, in Fig. 3) between the outcrop and the Santiago's gravel. This area does not have enough information to define a Vs model based on measurements; however, there are some Vs30s indicating Vs values greater than the northern fine soils and lower

than the Santiago's gravel. To model the variation of Vs with depth for gravel, fine soils, and the transition zone, we consider Eq. 1, proposed by Pilz et al. (2011), where V_s0 is the shear wave velocity in the surface and 〖dV〗_s is the rate of increase of the Vs in depth, we adjusted these parameters to get a good fit with de measured shear wave velocity profiles.

$$V_s = V_{s0} + dV_s \cdot \sqrt{\frac{Z}{1m}} \quad (1)$$

The Vs of shallow ignimbrites present in EW and CD cross-sections described in Fig. 2 were considered with a constant value of 350 m/s and 500 m/s for the deep layer of the EW cross-section, following Vs values reported by Lagos (2003).The P-wave velocity was estimated based on Eq. 2, proposed by Kitsunezaki et al. (1990), assuming that the soil has a high degree of saturation based on the low depths, between 0 and 15 m, of the groundwater level in the predominantly fine soils of the northwest area reported by Muñoz (2015). This assumption was no longer valid in the southeast area, where the maximum depths of the groundwater level reach 150 m, causing overestimation of P wave velocities. Nonetheless, this overestimation in the stiff Santiago's gravel does not affect the relative amplification of the horizontal with respect to the vertical within the studied frequency range.

$$V_p = 1.11 \cdot V_s + 1290 \quad (2)$$

The attenuation factors for the S and P-waves were estimated according to Eq. 3 and Eq. 4 (Makra et al. 2016).

$$Q_s = \frac{V_s}{10} \quad (3)$$

$$Q_p = 2 \cdot Q_s \quad (4)$$

The parameters adopted for Eq. 1 that best fit recently measured Vs profiles in the basin are shown in Table 1. The density of the materials was selected based on the reference values reported by Bonnefoy-Claudet et al. (2009).

Table 1 Dynamic soil parameters.

Soil type	Vs0 (m/s)	dVs (m/s)	Density (kg/m3)
Gravel	380	70	2100
Clayey sand	300	70	2100
Gravel and clay	300	70	2000
Sandy clay	300	70	1900
Clayey Gravel	300	70	1900
Silty clay	200	30	1600

We considered the Vs of the bedrock according to the seismic noise tomography developed by Salomon (2017). The cross-sections discretize the bedrock into 5 layers that vary their Vs gradually with depth: Vs= 1900 m/s for the first 500 m, Vs=2200 m/s for depths between 500 and 1000 m, Vs= 2800 m/s for depths between 1000 and 2000 m, Vs= 3100 m/s for depths between 2000 and 3000 m, and Vs=3400 m/s for depths greater than 3000 m. Finally, the cross-sections analyzed in this study are shown in Fig. 3. The top panels in each cross-section show the geological models and the bottom panels show the Vs models.

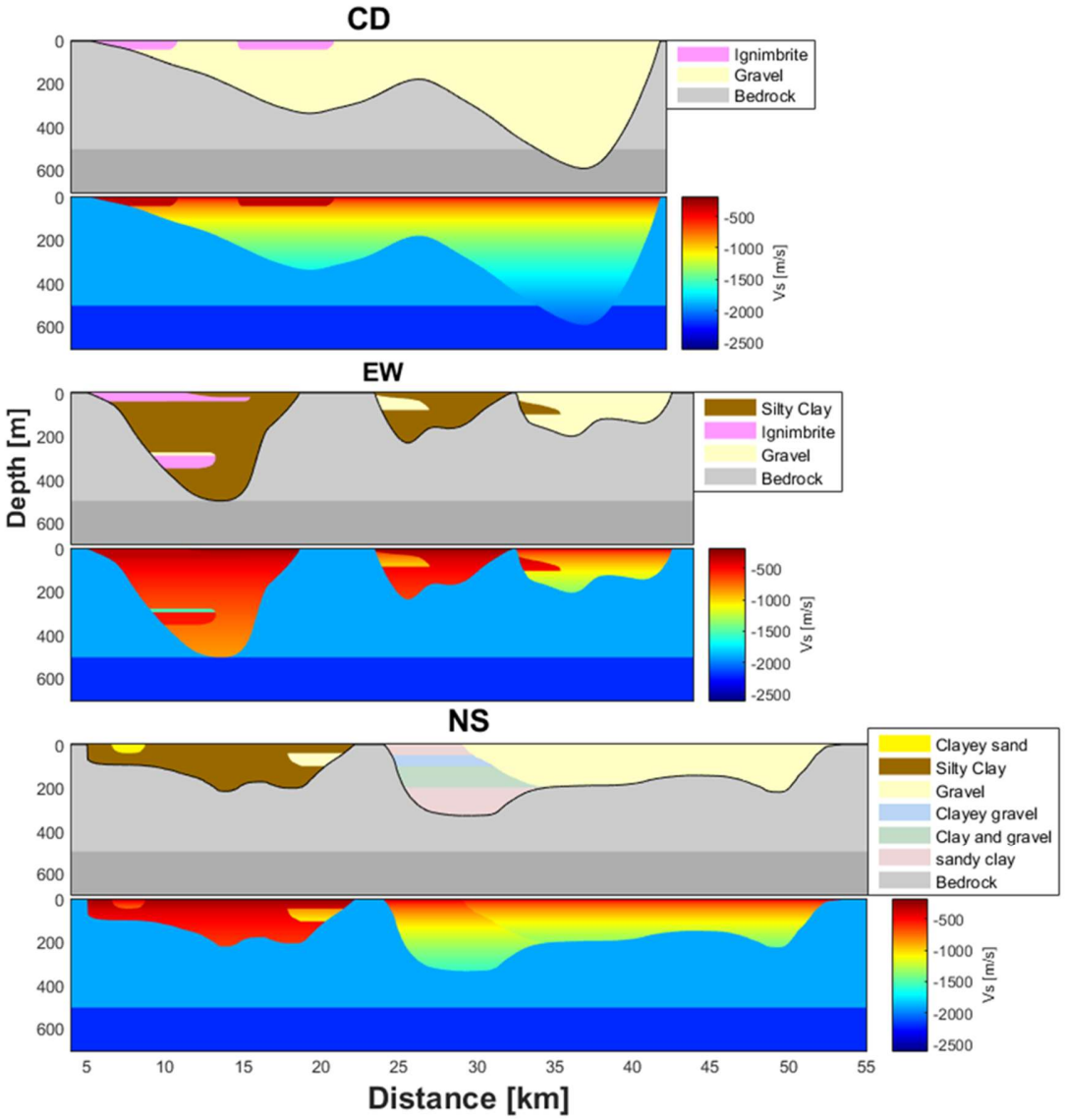

Figure 3 CD, EW, and NS cross-sections with the geological information at the top panels and the variation of Vs along the section at the bottom panels.

3.3 Numerical Simulations

Each cross-section was executed three times with 2D incident wavefronts: vertical P-wave wave-front (P), in-plane S-wave wavefront (SV), and out-plane S-wave wave-front (SH). In addition, two 1D simulations of the cross-sections are performed, vertical P-wave and S-wave wave-fronts.

Simulations allow retrieving the 2D response matrix shown in Eq 5. Paolucci (1999) showed that the response of 2D P-wave (r_{Pz} & r_{Px}) and 2D S-wave (r_{SVx} & r_{SVz}) input wavefronts can be superposed since the materials constitutive models are viscoelastic, and mention that terms outside the diagonal can be significant by introducing pure 2D effects. Finally, the 2D synthetic response in the longitudinal (R_x), transverse (R_y), and vertical (R_z) directions are given by Eq. 6, 7 & 8, respectively.

$$R_{2D} \equiv \begin{bmatrix} r_{SVx} & 0 & r_{Px} \\ 0 & r_{SHy} & 0 \\ r_{SVz} & 0 & r_{Pz} \end{bmatrix} \tag{5}$$

$$R_x = r_{SVx} + r_{Px} \tag{6}$$

$$R_y = r_{SHy} \tag{7}$$

$$R_z = r_{Pz} + r_{SVz} \tag{8}$$

Numerical simulations were performed using the finite difference code 2DFD_DVS (Moczo and Kristek 2007). This code allows the propagation of waves in a heterogeneous and viscoelastic medium. The constitutive model of the materials corresponds to the generalized Maxwell body. The boundary conditions used correspond to Emmerman and Stephen (1983) with maximum attenuation for P-waves and S-Waves.

The model had a depth of 10 km, with a grid defined by a spacing Δh= 5 m, which allows sufficient precision up to 5 Hz, considering that the minimum wavelength should be at least 8 spacings of the grid. The defined time step to ensure numerical stability is $\Delta t=5 \cdot 10^{-4}$ s. The source is located at 5 km depth in all models and the source function adopted in this study is a Gabor pulse with the following parameters: $f_p = \frac{\omega_p}{2\pi} = 0.18\,Hz$, $\gamma = 0.2$, $\theta = 0.0$, and $t_s = 0.45 \cdot \frac{\gamma}{f_p}$. The pulse has energy up to 5 Hz and its similar to other studies (Chávez-García 2003; Kristek et al. 2018).

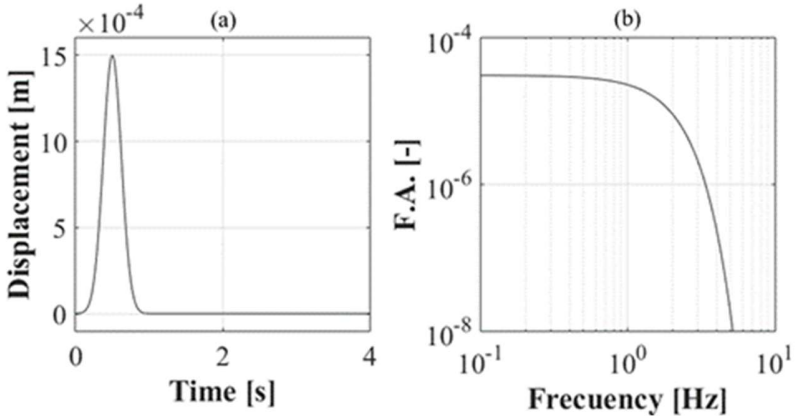

Figure 4 Gabor pulse adopted as source function is shown in (a), (b) shows the Fourier amplitude of the source function.

Chapter 4

Results

4.1 Surface ground motion

Fig. 5 shows the particle velocity at the surface of the models in the horizontal component for the S-wave wavefront in 1D, 2D “in-plane,” and 2D “out of plane” cases, for the three cross-section models. Red signatures show the time lapse between the first and the last time that the surface velocity exceeds 30% of the peak ground velocity (PGV) in the outcrop.

In the CD cross-section, there are no significant differences between the 1D and 2D wave propagation. This is mainly because this cross-section consists of Santiago’s gravel of high stiffness. However, areas with presence of ignimbrites of lower Vs, experience an elongation of the strong motion phase. In the EW cross-section, a significant increase in the of the strong motion duration can be observed in areas with softer soils, and this effect was more pronounced in the deepest sediments. In the east area of the model filled with Santiago gravel, the seismic behavior was similar to the CD model, except in the SH case that was strongly influenced by the refraction of waves on the west boundary. Finally, the NS cross-section confirms the effects described in the CD and EW cross-sections. The southern area of the NS cross-section ranging from 23 to 53 km, composed of rigid to very rigid soils, show slight differences between the 1D and 2D simulations. On the other hand, the northern area composed mainly of soft soils shows an elongation of the strong motion duration in 2D simulations not as severe as the EW cross-section, because the deposits are considerably shallower.

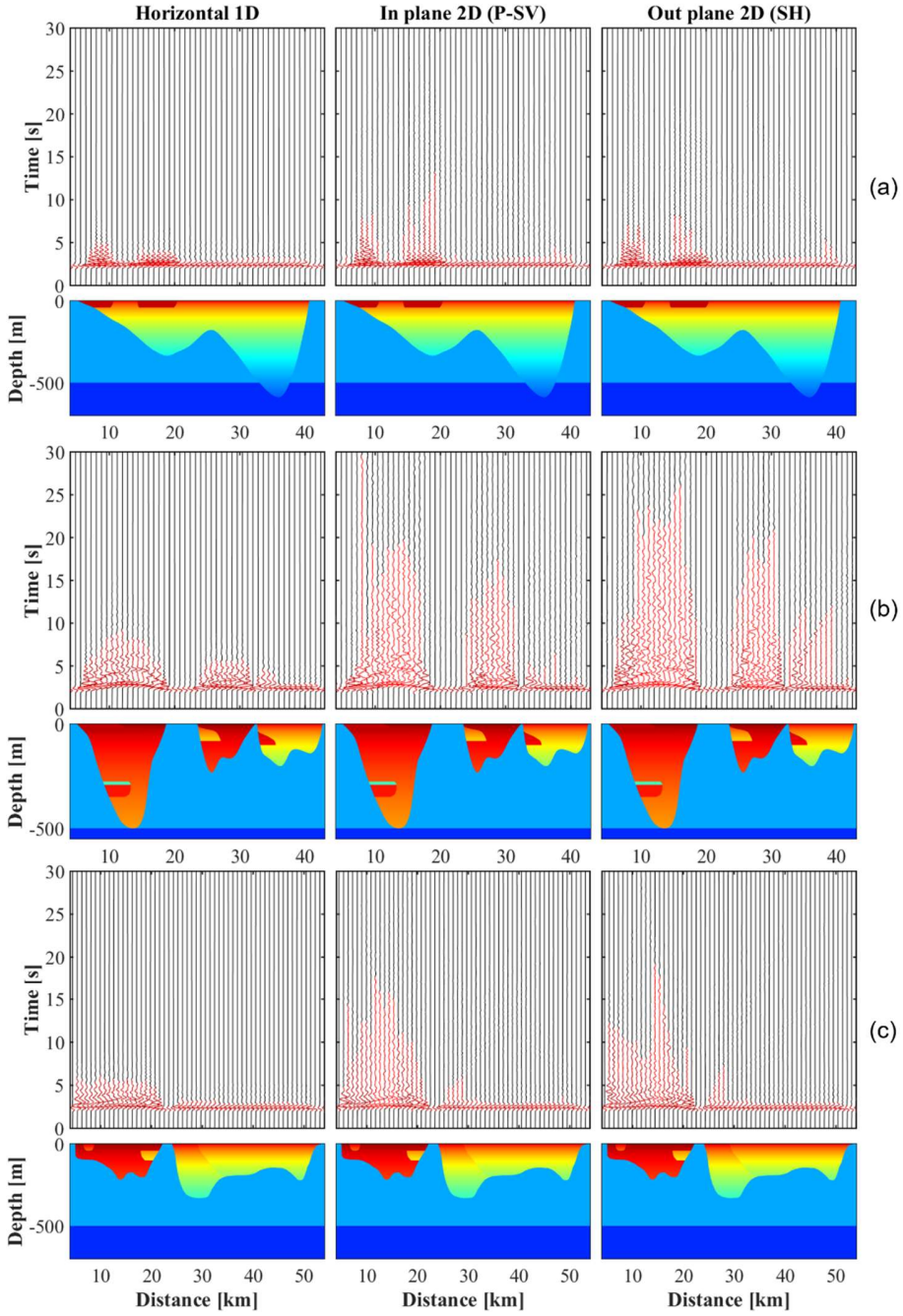

Figure 5 Surface ground motion in each cross-section, in the left column is shown the 1D case, the central column shows the 2D SV in-plane case and the right column shows de 2D SH out-plane case. (a) CD cross-section, (b) EW cross-section and (c) NS cross-section.

4.2 H/V Spectral Ratios (HVSR)

We analyzed HVSRs instead of Fourier spectral ratios amplitudes since the last type of analysis is limited to study the dynamic response in each direction separately because it is necessary to define a reference site in outcrop. On the other hand, calculation of HVSRs allows analyzing the response of the site considering the superimposed directions. In this way, it is possible to compare the synthetic response generated by 2D models with records of seismic events. HVSR was calculated on surface receivers throughout each cross-section. HVSR was calculated by dividing the Fourier's spectral amplitude of the superposed horizontal component of the model by the Fourier's spectral amplitude of the superimposed vertical response. The Fourier's spectral amplitude was calculated considering 30 seconds of the synthetic record. Fig. 6 shows the predominant frequencies and their respective peak amplitude for each HVSR calculated along the surface of each cross-section. Stiff soils have amplitudes lower than 2.0 without the presence of a clear peak. Softer soils have considerably higher amplitudes, and their predominant frequencies are inversely related with the depth of the bedrock. By comparing 1D and 2D analyses, it is noted there are no major differences in the predominant frequencies of each site, but there are areas where the HVSR amplitudes can vary significantly. These differences occur mainly in areas with strong spatial variations in the dynamic soil properties. An example is the shallow boundaries between outcrop and soft soils, where 1D models tend to overestimate the amplitude of the HVSR peaks compared to 2D models.

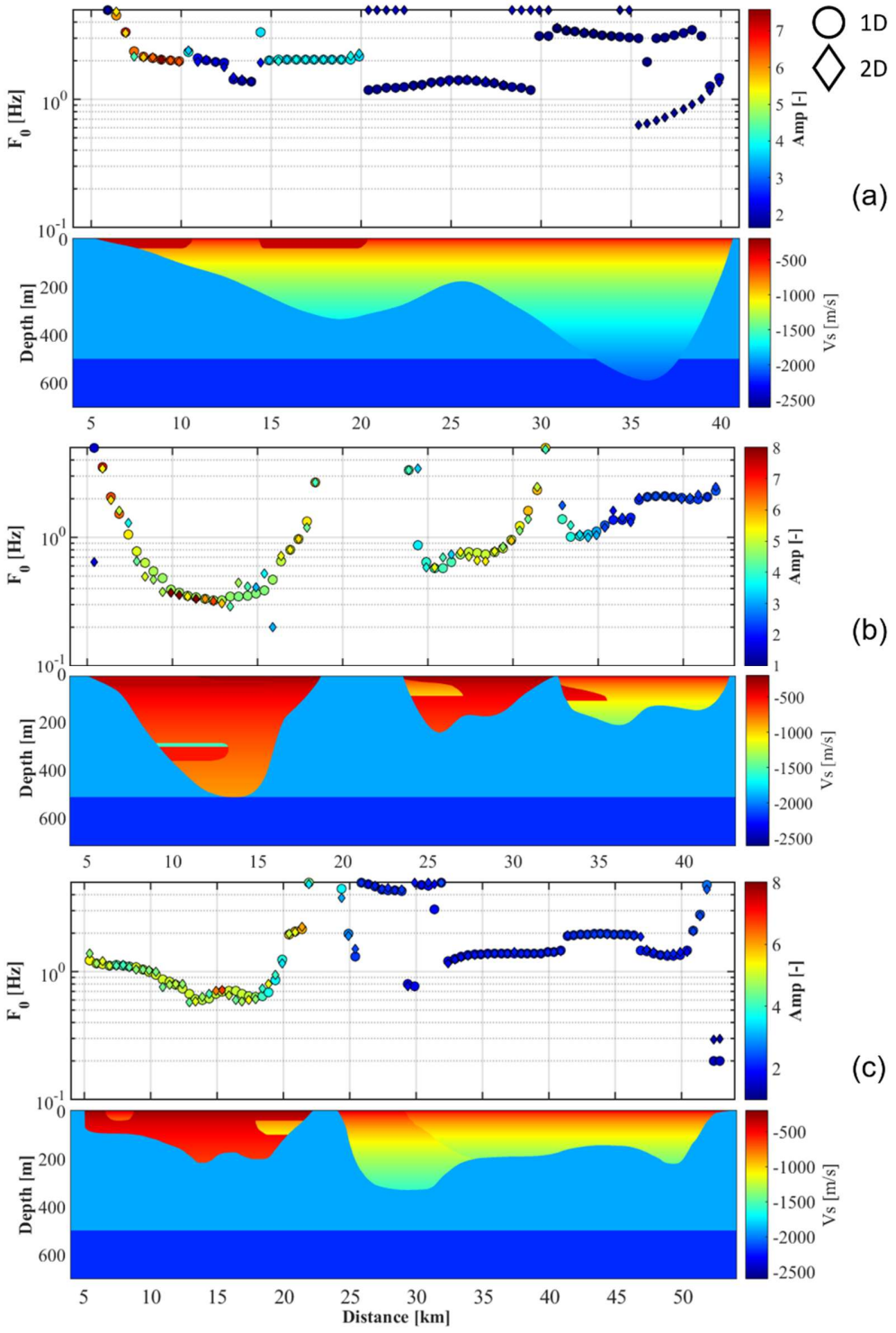

Figure 6 HVSR in the surface of each cross-section. (a) CD cross-section, (b) EW cross-section and (c) NS cross-section.

4.3 Amplification and aggravation factors

To understand the surface amplification patterns throughout the models and following the study of Kristek et al. (2018), amplification factors (*AF*s) and aggravation factors (*AGF*s) are calculated for different earthquake ground motion characteristics (*EGMC*s). The *EGMC*s selected for this study are the *PGV*, the Cumulative Absolute Velocity (*CAV*), and the Arias Intensity (*AI*). More information about these EGCMs can be found in Kramer (1996).

The *AF* was calculated as the ratio of the *EGMC* value in each surface receptor and the EGMC value on the rock outcrop. Fig. 7, 8 & 9 show *AF* along CD, EW, and NS cross-sections for each *EGMC* in the vertical, in-plane, and out-plane directions for 1D and 2D analyses. *PGV* amplification factors are lower than 2 in the vertical direction. Horizontal amplification values (in-plane and out-plane) are close to 2 in areas with stiffer soils, whereas horizontal amplification factors can reach values up to 4 in areas with softer soils. *CAV* amplification factors are higher in the vertical component compared to the *AF* of the *PGV,* these differences were mainly because of the arrival of the S-wave front that generates larger amplitude surface waves that considerably extend the phase of strong movement especially in soils with low *Vs* values. In the horizontal components, the amplification patterns of the *PGV* case are maintained because both duration and maximum amplitude are related to the arrival of the S-wave front. *AI* amplification factors are considerably higher than those of the *PGV* and *CAV* due to strong impedance contrasts between softer soils and the bedrock and strong spatial variations near the boundaries of the basin.

The *AGF* was calculated as the ratio of the AF value for 2D analysis by the *AF* value of the 1D analysis. Note that *AGF*s for each EGMC are calculated. Fig. 10,11 & 12 shows the *AGF*s calculated along CD, EW, and NS cross-sections for each *EGMC* in the vertical, in-plane, and out-plane directions. *AGF* of *PGV* shows that there are no significant differences between 1D and 2D models. *CAV* and *AI* are *EGMC*s strongly related to the time variable, so these *AGF*s show greater *AF* values in 2D than 1D analyses. These differences are chiefly associated with the duration of the strong motion captured by 2D models, which is not considered by 1D models.

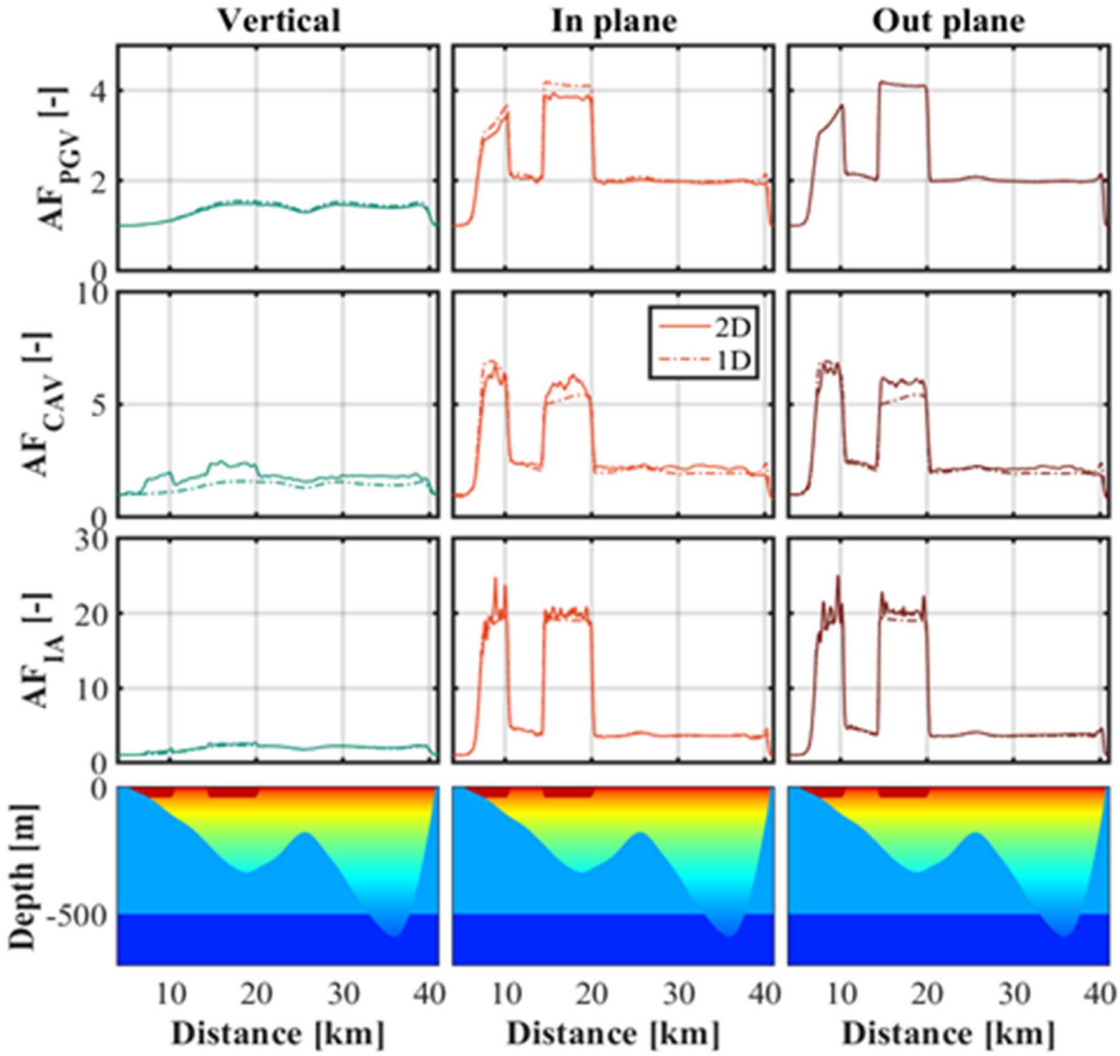

Figure 7 Amplification factors for PGV (upper panels), CAV (center panels) and IA (lower panels) along the CD cross-section.

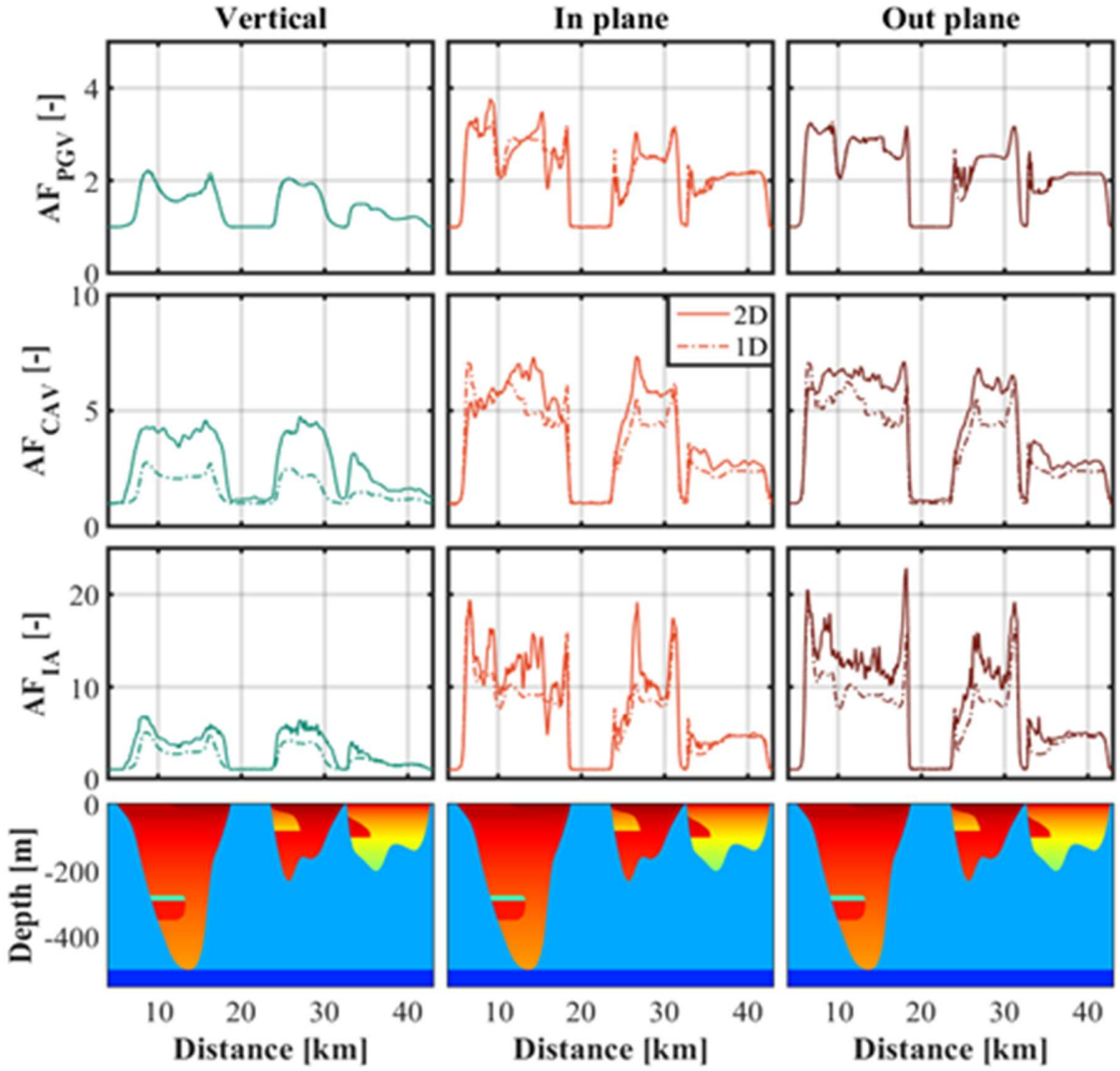

Figure 8 Amplification factors for PGV (upper panels), CAV (center panels) and IA (lower panels) along the EW cross-section.

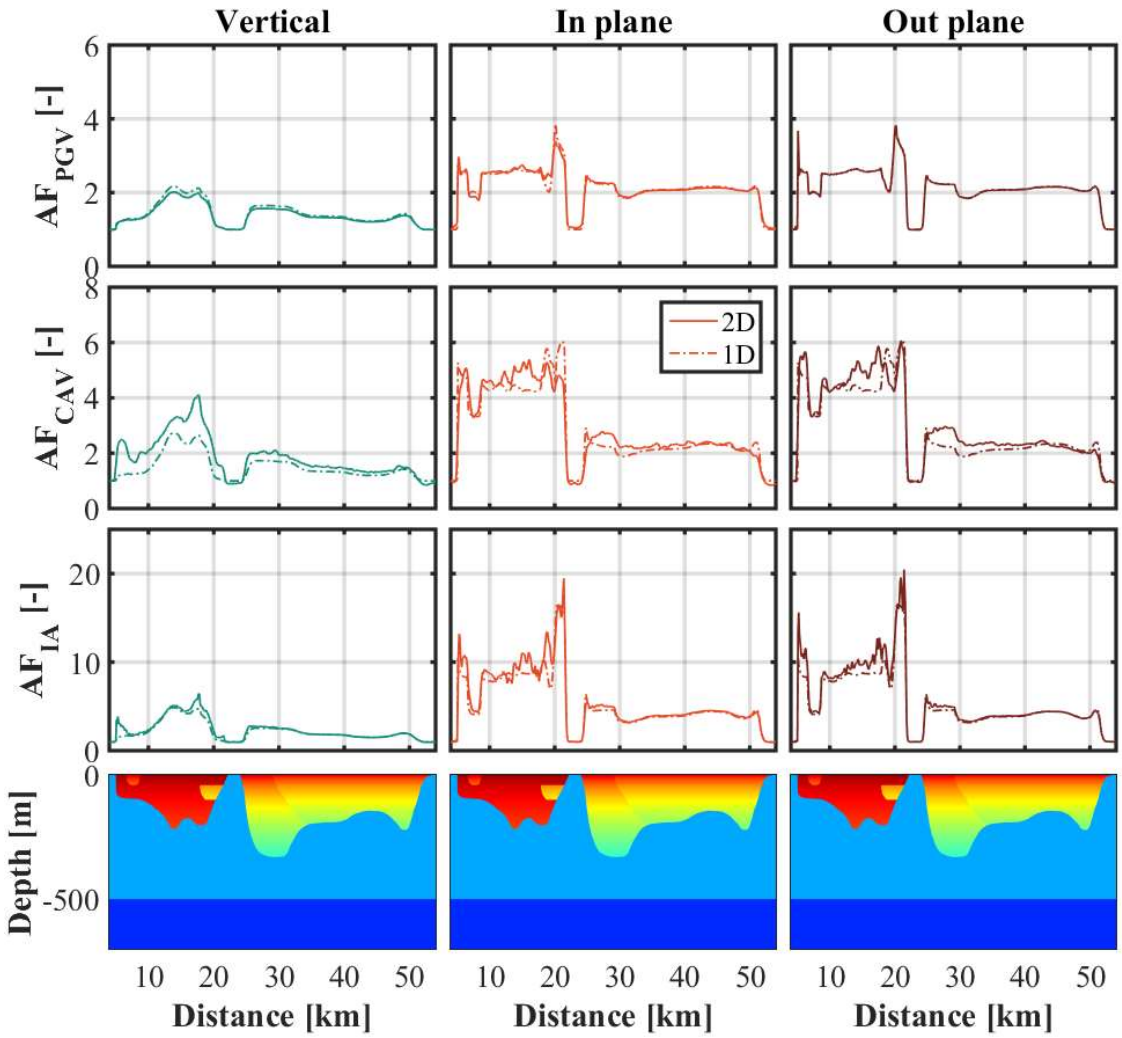

Figure 9 Amplification factors for PGV (upper panels), CAV (center panels) and IA (lower panels) along the NS cross-section.

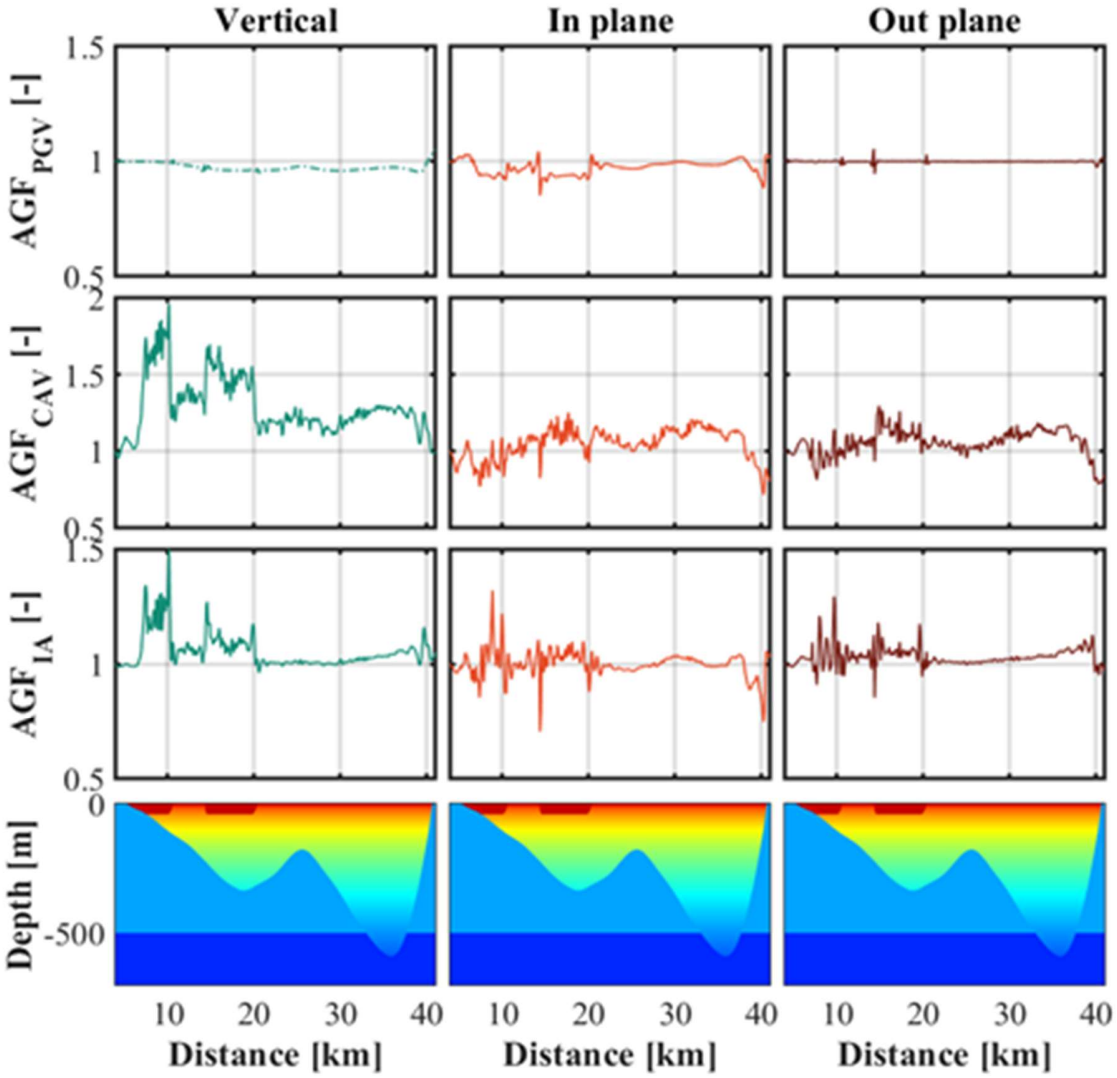

Figure 10 PGV, CAV and IA, Aggravation factors for CD cross-section.

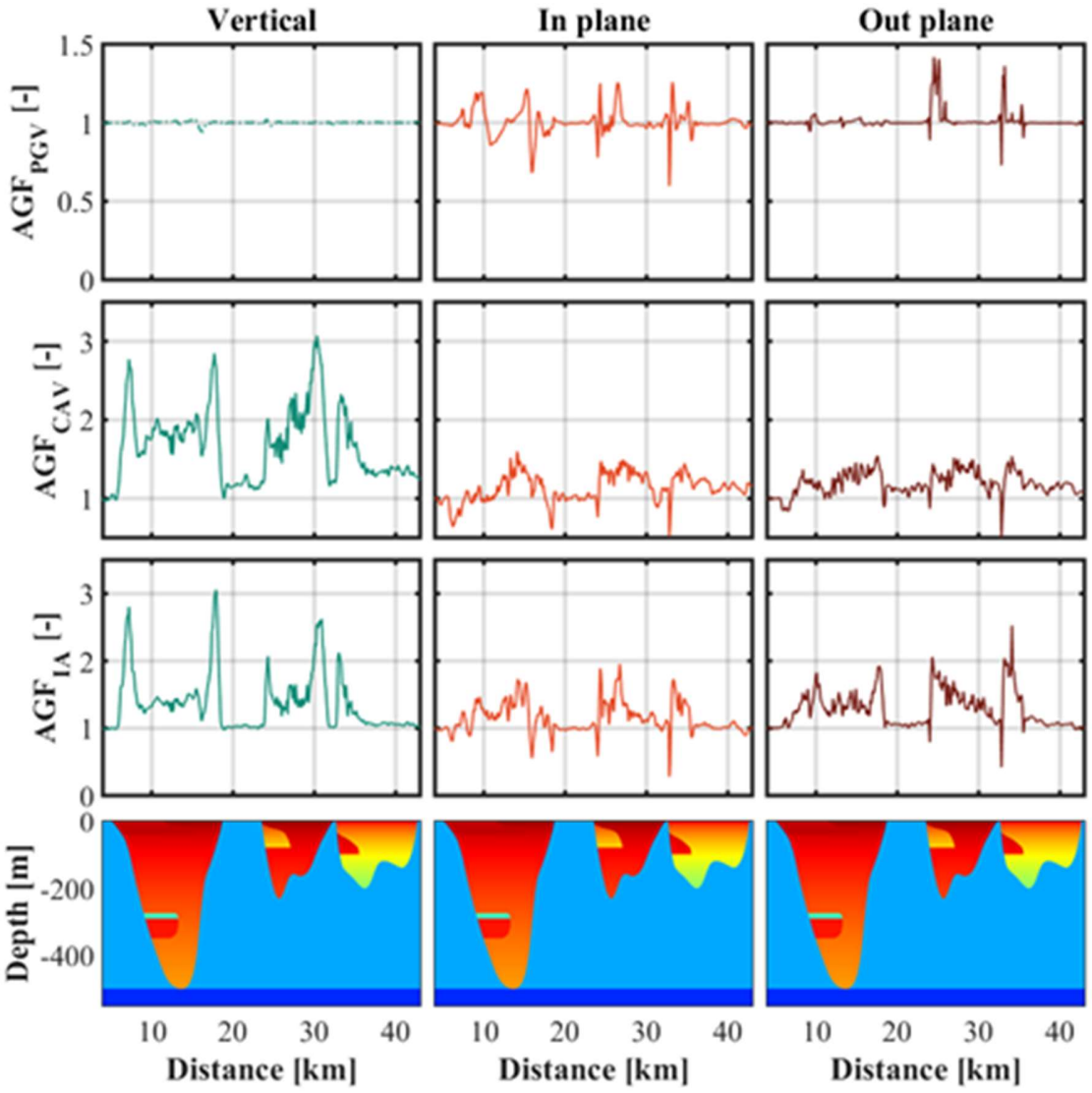

Figure 11 PGV, CAV and IA, Aggravation factors for EW cross-section.

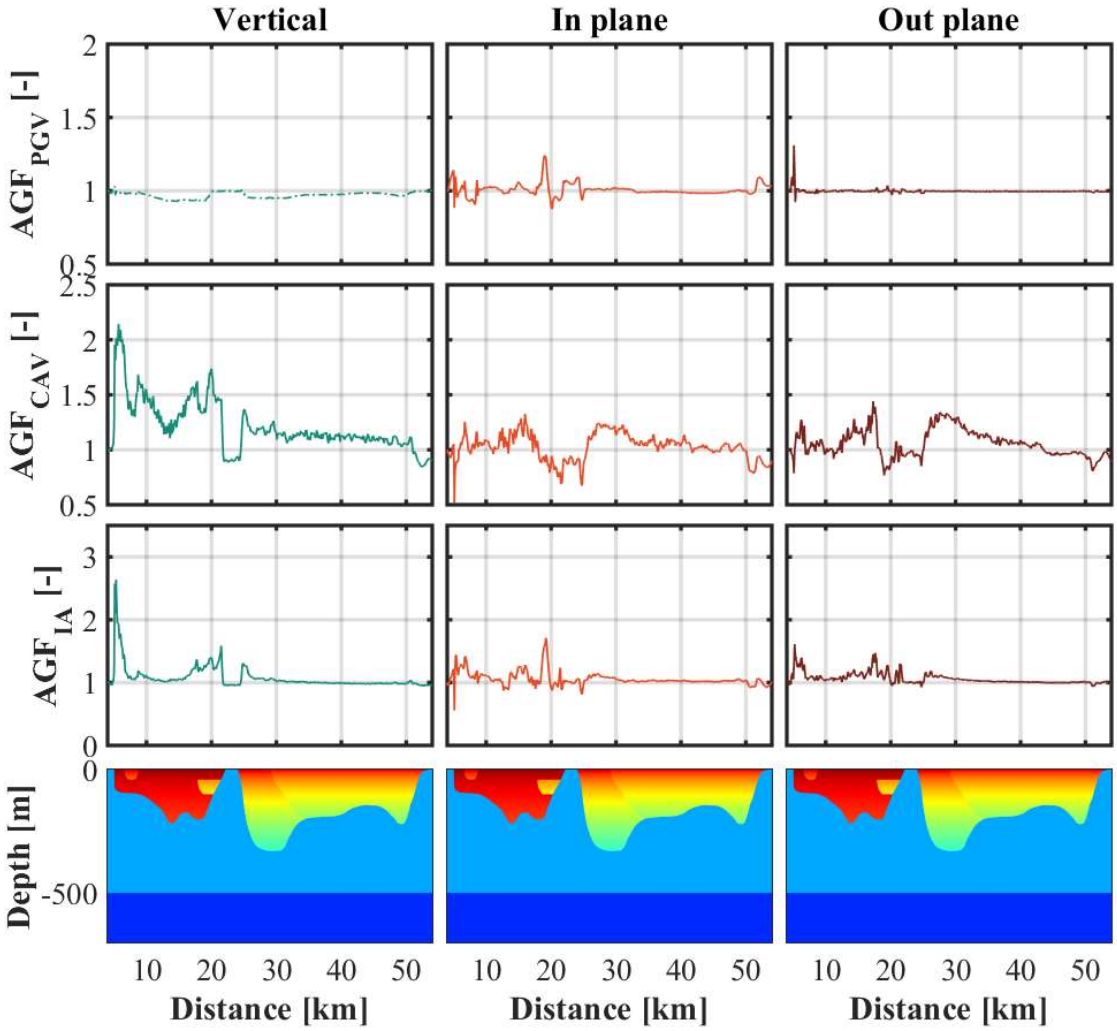

Figure 12 PGV, CAV and IA, Aggravation factors for NS cross-section.

Chapter 5 :

Empirical Evidence of Seismic Amplification

5.1 Empirical Evidence of Seismic Amplification

The last large earthquake that affected the urban area of the city of Santiago was the 2015 Mw 8.3 Illapel Earthquake. This event occurred at approximately 220 km north of Santiago and was recorded by several accelerographs of the National Seismological Center (CSN) along with the CD, and EW cross-section of the basin (Fig. 1). To compare the evidence of seismic amplification with the numerical models presented herein, we focus on six seismic stations. R12M, R14M, and R21M located along the EW cross-section, and R18M, R02M, and R22M located along the CD cross-section. To compare seismic records with synthetic records obtained from the developed 2D numerical models, we define the relative Peak Ground Acceleration (PGA_r) and relative Arias Intensity (AI_r), which are calculated as the ratio between each value of the record and the lowest value of all analyzed records. The seismic records, PGA_r and AI_r in the north-south, east-west, and vertical directions are shown in Fig. 13. The records were bandpass filtered between 0.1 and 3.5 Hz to make them comparable with the synthetic records obtained from numerical models. Stations R12M and R21M, located over the northern fine-grained soils (unit VII, Fig. 1), and station R18M, located over the pumice deposits (unit VI, Fig. 1), show larger amplitudes than those of the stations R02M, R14M, and R22M, located over Santiago gravel (unit II, Fig. 1).

PGA_r and AI_r show a similar seismic response at R02M, R14M, and R22M stations, located over Santiago gravel. On the other hand, stations R12M, R18M, and R21M, located over softer soils, show values considerably higher.

HVSRs of the records in Fig. 15 show that station R12M has a predominant frequency of 1.1 Hz, station R18M shows amplification effects of the horizontal component between 2 and 3 Hz with a predominant frequency of 2.5 Hz. On the other hand, station R21M has a predominant frequency at 0.3 Hz, while the *HVSRs* of stations R02M, R14M, and R22M, tend to be flat because they are placed on Santiago's gravel.

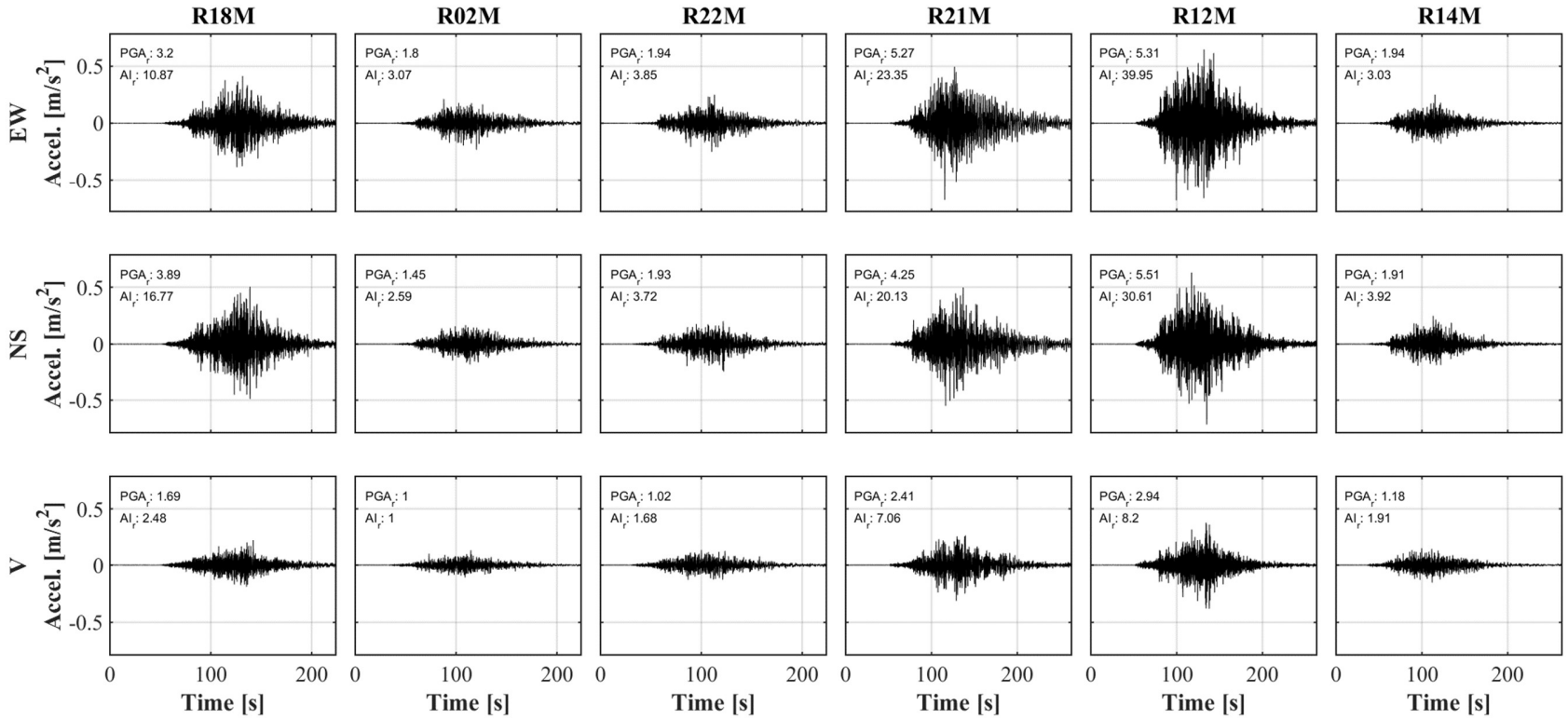

Figure 13 Seismic records obtained at stations R18M, R02M, R22M, R21M, R12M and R14M, for the Illapel 2015 Mw 8.4 earthquake. Peak Ground Acceleration (PGA_r) and relative Arias Intensity (AI_r) are calculated as the ratio between each value of the record and the lowest value of all analyzed records.

5.2 Comparison with seismic evidence in the CD, and EW cross-section

The receptors of the CD and EW cross-sections closest to the R02M, R12M, R14M, R18M, R21M, and R22M stations are selected to compare the numerical results with the seismic evidence presented above. Fig. 14 shows the synthetic records of each station in each direction. The EW direction corresponds to the in-plane component and the NS direction corresponds to the out-plane component.

The synthetic records present similar relative amplitudes with the seismic records for the stations R02M, R14M, R18M, and R22M. Seismic records of stations R21M and R12M present considerably higher relative amplitudes than synthetic records, However, synthetic records are able to capture the amplification patterns observed during the 2015 Mw 8.3 Illapel earthquake.

Finally, we compared the *HVSR*s of seismic records with the synthetic records following the same calculation procedure. Fig. 15 shows in black the *HVSR* of the seismic records, and in red the *HVSR* of the synthetic records obtained from the 2D model. Stations R02M, R14M, and R22M, located over Santiago gravel, show flat *HVSR*s in both, seismic and synthetic records. Synthetic *HVSR* tends to slightly underestimate the predominant frequency and the amplitude peak of the R18M station. The synthetic *HVSR* of the R21M and R12M stations can capture the predominant frequency of the deposits more precisely, but the underestimation of the peak amplitude was also observed. The receptors of the CD and EW cross-section closest to the R02M, R12M, R14M, R18M, R21M, and R22M stations are selected to compare the numerical results with the seismic evidence presented above. Fig. 14 shows the synthetic records of each station in each direction. The EW direction corresponds to the in-plane component, and the NS direction corresponds to the out-plane component.

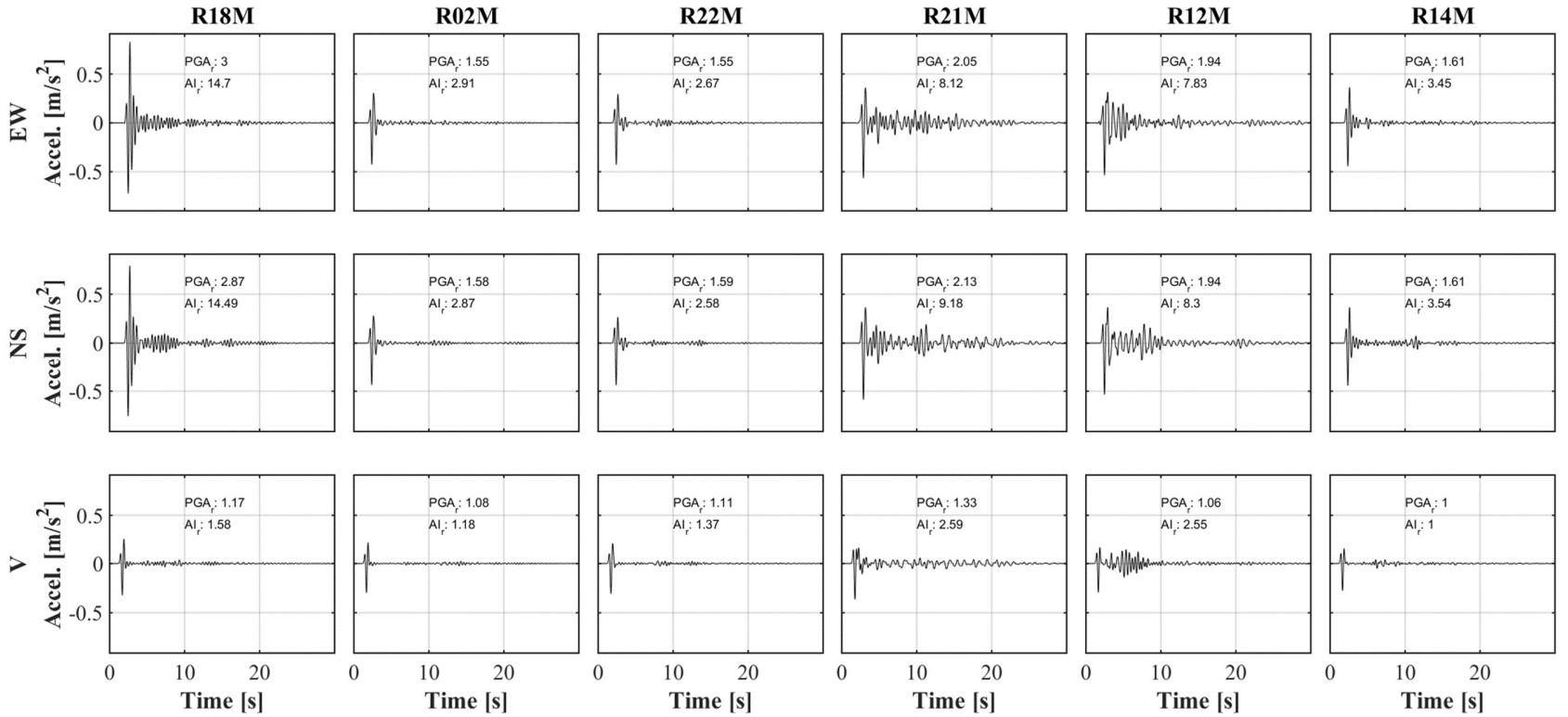

Figure 14 Synthetic records obtained at stations R18M, R02M, R22M, R21M, R12M and R14M. EW direction corresponds to the in-plane component and NS direction corresponds to the out-plane component.

.

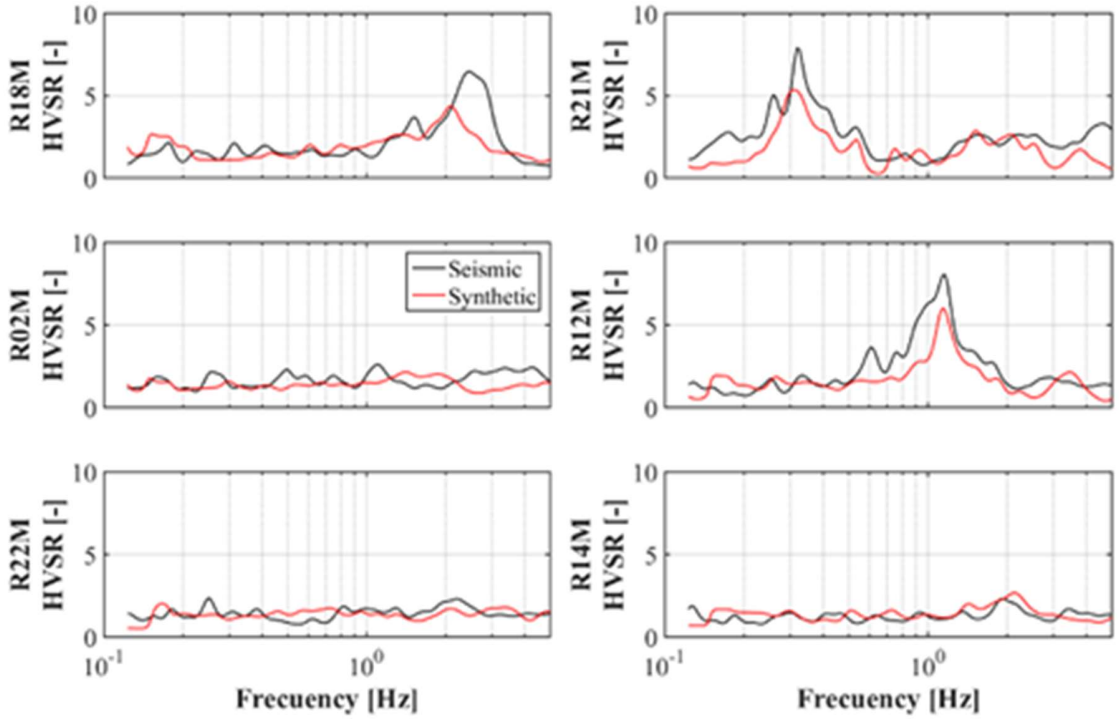

Figure 15 HVSR comparison between seismic and synthetic records.

Chapter 6 :

Discussion and Conclusions

6.1 Discussion

From the 2D numerical models of the three cross-sections investigated in this study, it can be noted that *HVSR* predominant frequencies in fine soils are well adjusted with respect to the seismic evidence presented. Numerical models underestimate the predominant frequency measured in Ignimbrites. In rigid soils, it was not possible to determine a predominant frequency because no significant amplitudes (usually lower than 3) are observed in *HVSR*s. The Vs model introduced in this study presents a good fit for the northern fine soils and Santiago's gravel; however, underestimation of the predominant frequency of ignimbrites indicates that the value of actual Vs is higher than that adopted in the model. To improve the modeling accuracy, more measurements are required in areas with low density of information, being one example, the transition zone defined in the NS cross-section.

When analyzing the results obtained from 2D numerical simulations and comparing them with 1D simulations, considering the superficial synthetic records, *HVSR*s, as well as aggravation and amplification factors, it was observed that stiff soils in the Santiago basin do not show significant differences in 1D and 2D amplification patterns. This effect may be associated with the low impedance contrast between the soil and the underlying bedrock, which hinders 2D effects generated by the bedrock geometry. On the other hand, 2D effects are clearly noticed in softer sediments and become even more pronounced as the depth of the deposits increases. The surface response of 2D simulations have considerably longer durations than those obtained in 1D models, mainly due to the generation of surface waves in 2D simulations in addition to the refraction and reflection effect of seismic waves. Areas with strong spatial variations of Vs generate the biggest differences between 1D and 2D simulations. This is directly related to the geometric stiffness that is incorporated in 2D models, specifically in the P-SV case involving vertical and longitudinal direction. In these areas, we observed considerable differences in the amplitudes of the HVSRs, predominant frequencies calculated had small variations associated with the geometry stiffening effect, and aggravation factors show large variations that even increase in shallow boundaries between the outcrop and softer soils, agreeing with the study developed by Zhu et al (2018).

The comparison between the synthetic response obtained from 2D simulations for the CD and EW cross-sections and the seismic records shows that R02M, R14M, and R22M stations, located on Santiago gravel, show similar seismic behavior, being consistent with synthetic amplification factors that are relatively constant in this soil type. *PGV* and *AI* of the seismic records show amplification patterns similar to the *AF* obtained. Finally, comparing *HVSR*s show similar predominant frequencies for R12M, R18M, and R21M stations, but synthetic records underestimate amplitudes. The R18M station located on ignimbrite show a lower synthetic predominant frequency, suggesting that the surface deposits of ignimbrites are stiffer than what assumed in the models.

The highest values of synthetic *PGV*s occur in the fine soils of the northwest area where the highest intensities were observed in the Valparaiso 1985, Maule 2010, and Illapel 2015 earthquakes, so we proposed that the variation of the intensity values in the Santiago basin are strongly controlled by the depth of the bedrock, the dynamic properties of the soils in-depth and the edge effects on the outcrops.

6.2 Conclusions

The numerical models developed show that the Santiago basin has important amplification effects in areas that have soft soils, generating an elongation of the strong motion, which becomes more pronounced in deeper deposits. These effects are not captured by 1D models because the duration of the strong motion is linked to refraction and reflection of waves, in addition to the generation of surface waves. On the other hand, 2D models can generate surface waves and capture bidimensional effects in a better way due to the superposition of the directions contained in the plane. Contrarily, rigid soils show no considerable amplification effects compared to fine soils and there are no large differences between 1D and 2D simulations, so it can be concluded that the rigid soils of the Santiago basin do not suffer appreciable two-dimensional effects.

The superposition of responses in the directions contained in the plane shows that the second-order effects generated by the S wavefront (r_{SVz}) has a considerable amplitude in softer deposits compared to the second-order effects generated by the P wavefront (r_{Px}), confirming the observations described by Paolucci (1999).

Aggravation factors show significant differences between 1D and 2D models when *EGMC*s involving time in their calculation (e.g., *CAV* and *AI*) are analyzed. This is due to the elongation of the strong motion generated by 2D models, differences observed mainly in fine soils.

The numerical results presented in this work are consistent with empirical evidence gathered from the 2015 Mw 8.3 Illapel earthquake records along the CD and EW cross-section. From this comparison, it was possible to observe that the same amplification patterns are generated, but, in general, with smaller amplitudes in the synthetic records. In the frequency domain, it was possible to observe a good agreement in the predominant frequencies in *HVSR*s of stations located on softer soils, while in stations located on stiffer soils, it was possible to obtain flat *HVSR*s as those calculated from empirical data.

6.3 Acknowledgements

Support for this research was provided by the FONDECYT project 1190995 and the National Laboratory for High Performance Computing (NLHPC). We would like to acknowledge the National Seismological Center (CSN) of the University of Chile for the data delivered.

Chapter 7 Bibliography

Araneda, M., Avendaño, M. y Merlo, C., 2000. Modelo gravimétrico de la cuenca de Santiago, etapa III final. IX Congreso Geológico de Chile, Puerto Varas, Chile, 2, 404-408.

Astroza, M., Ruiz, S., Astroza, R., 2012. Damage assessment and seismic intensity analysis of the 2010 (Mw 8.8) maule earthquake. Earthq. Spectra 28, 145–164. https://doi.org/10.1193/1.4000027

Bonnefoy-Claudet, S., Baize, S., Bonilla, L.F., Berge-Thierry, C., Pasten, C., Campos, J., Volant, P., Verdugo, R., 2009. Site effect evaluation in the basin of Santiago de Chile using ambient noise measurements. Geophys. J. Int. 176 (3), 925–937.

Chávez-García, F.J., 2003. Site effects in Parkway Basin: comparison between observations and 3-D modelling. Geophys. J. Int., 154, 633-646.

Ekström, G., 2014. Love and Rayleigh phase-velocity maps, 5-40 s, of the western and central USA from USArray data. Earth Planet. Sci. Lett. 402, 42–49. https://doi.org/10.1016/j.epsl.2013.11.022

Ekström, G., Abers, G. a., Webb, S.C., 2009. Determination of surface-wave phase velocities across USArray from noise and Aki's spectral formulation. Geophys. Res. Lett. 36, 5–9. https://doi.org/10.1029/2009GL039131

Emerman, S.H., and Stephen, R.A., 1983, Comment on "absorbing boundary conditions for acoustic and elastic wave equations", by R. Clayton and B. Engquist: Bull. Seism. Soc. am., 73, 661-665.

Fernández, J.C. (2001). Estudio geológico-ambiental para la planificación territorial del sector Tiltil - Santiago. Memoria de título, Universidad de Chile

Fernández, J.C. (2003). Respuesta sísmica de la cuenca de Santiago. Servicio Nacional de Geología y Minería. Carta Geológica de Chile. Serie Geología Ambiental N°1.

Fock, A., 2005. Cronología y tectónica de la exhumación en el Neógeno de los Andes de Chile central entre los 33° y los 34°S. Tesis para optar al grado de Magister en Ciencias de la Ingeniería, mención Geología. Departamento de Geología, Universidad de Chile.

Gálvez, C., 2012. Microzonificación sísmica en los sectores de Lampa y Batuco, Región Metropolitana, Chile. Memoria para optar al título de Geólogo. Departamento de Geología, Universidad de Chile.

González, F.A., Maksymowicz, A., Díaz, D., Villegas, L., Leiva, M., Blanco, B., Vera,

E., Contreras, S., Cabrera, D., Bonvalot, S., 2018. Characterization of the depocenters and the basement structure, below the central Chile Andean Forearc: A 3D geophysical modelling in Santiago Basin area. Basin Res. 30, 799–815. https://doi.org/10.1111/bre.12281

Hobiger, M., Bard, P. Y., Cornou, C., & Le Bihan, N. (2009). Single station determination of Rayleigh wave ellipticity by using the random decrement technique (RayDec). Geophysical Research Letters, 36(14).

Hobiger, M., Cornou, C., Wathelet, M., Giulio, G. D., Knapmeyer-Endrun, B., Renalier, F., ... & Theodoulidis, N. (2013). Ground structure imaging by inversions of Rayleigh wave ellipticity: sensitivity analysis and application to European strong-motion sites. Geophysical Journal International, 192(1), 207-229.

Kitsunezaki, N., Noritoshi, G., Yoshimasa, K., Takeshi, I., Masanori, H., Tokumi, S., Toru, K., Kazunobu, Y. & Koichi, O., 1990. Estimaton of P- and S-Wave Velocities in Deep Soil Deposits for Evaluating Ground Vibrations in Earthquake. Japan Society for Natural Disaster Science, 9, 1-17.

Kramer, S. L. (1996). Geotechnical earthquake engineering. Upper Saddle River, N.J: Prentice Hall.

Kristek, J., Moczo, P.,Bard, P.-Y., Hollender, F. & Stripajová, S. 2018. Computation of amplification factor of earthquake ground motion for a local sedimentary structure. Bull. Earthquake Eng.

Lagos, J., 2003. Ignimbrita Pudahuel: caracterización geológico-geotécnica orientada a su respuesta sísmica. Memoria para optar al título de Geólogo. Departamento de Geología. Universidad de Chile.

Leyton, F., Sepúlveda, S. A., Astroza, M., Rebolledo, S., Acevedo, P., Ruiz, S., ... & Foncea, C. (2011, January). Seismic zonation of the Santiago basin, Chile. In 5th International Conference on Earthquake Geotechnical Engineering.

Makra, K., Chávez-García, F.J., 2016. Site effects in 3D basin using 1D and 2D models: an evaluation of the differences based on simulations of the seismic response of Euroseistest. Bull Earthq. Eng 14, 1177–1194. https://doi.org/10.1007/s10518-015-9862-7

Milovic, J.J. (2000). Estudio geológico-ambiental para el ordenamiento territorial de la mitad sur de la cuenca de Santiago. Memoria de título, Universidad de Concepción

Moczo, P., Kristek, J., Bard, P.-Y., Stripajová, S., Hollender, F., Chovanová, Z., Kristeková, M., Sicilia, D., 2018. Key structural parameters affecting earthquake ground motion in 2D and 3D sedimentary structures. Bull. Earthq. Eng. https://doi.org/10.1007/s10518-018-0345-5

Moczo, P., Kristek, J., Galis, M., Pazak, P., Balazovjech, M., 2007. The Finite-Difference and Finite-Element Modeling of Seismic Wave Propagation and Earthquake Motion. Acta Physica Slovaca 57, 177-406.

Monge, J., Astroza, M., 1989. Metodología para determinar el grado de intensidad a partir de los daños. V Jornadas Chilenas de Sismología e Ingeniería Antisísmica. Vol. 1, pp. 483-49.

Muñoz, M., Garat, P., Flores Aqueveque, V., Vargas Easton, V., Rebolledo Lemus, S., Sepúlveda Valenzuela, S., Daniele, L., Morata Céspedes, D. y Parada Reyes, M. (2015).Estimating low-enthalpy geothermal energy potential for district heating in Santiago basin-Chile (33.5 degrees S). http://repositorio.uchile.cl/handle/2250/133168

Pastén, C., 2007. Respuesta sísmica de la cuenca de Santiago. Tesis para optar al grado de Magister en Ciencias de la Ingeniería, mención Ingeniería Geotécnica. Departamento de Ingeniería Civil, Universidad de Chile.

Pastén, C., Sáez, M., Ruiz, S., Leyton, F., Salomón, J., Poli, P., 2016. Deep characterization of the Santiago Basin using HVSR and cross-correlation of ambient seismic noise. Eng. Geol. 201, 57–66. https://doi.org/10.1016/j.enggeo.2015.12.021

Pavez Carrillo, D. (2020).Modelamiento dinámico de perfiles geotécnicos bidimensionales de gran escala en la Cuenca de Santiago. Disponible en http://repositorio.uchile.cl/handle/2250/177318

Pilz, M., Parolai, S., Picozzi, M., Wang, R., Leyton, F., Campos, J., Zschau, J., 2010. Shear wave velocity model of the Santiago de Chile basin derived from ambient noise measurements: A comparison of proxies for seismic site conditions and amplification. Geophys. J. Int. 182, 355–367. https://doi.org/10.1111/j.1365-246X.2010.04613.x

Pilz, M., Parolai, S., Stupazzini, M., Paolucci, R., Zschau, J., 2011. Modelling basin effects on earthquake ground motion in the Santiago de Chile basin by a spectral element code. Geophysical Journal International, 187(2), 929-945.

Rauld, R. (2002). Análisis morfoestructural del frente cordillerano Santiago Oriente, entre el río Mapocho y quebrada de Macul. Memoria de título, Universidad de Chile

Ruiz, S., & Madariaga, R. (2018). Historical and recent large megathrust earthquakes in Chile. Tectonophysics, 733, 37-56.

Salomón, J., 2017. Tomografía de ruido sísmico de la cuenca de Santiago. Tesis para optar al grado de Magister en Ciencias de la Ingeniería, mención Ingeniería Estructura, Sísmica y Geotécnica. Departamento de Ingeniería Civil, Universidad de Chile.

Sellés, D., Gana, P., 2001. Geología del área Talagante-San Francisco de Mostazal: región metropolitana de Santiago y del Libertador general Bernardo O'Higgins. Servicio Nacional de Geología y Minería.

Vergara, Loreto, & Verdugo, Ramón. (2015). Condiciones geológicas-geotécnicas de la cuenca de Santiago y su relación con la distribución de daños del terremoto del 27F. Obras y proyectos, (17), 52-59. https://dx.doi.org/10.4067/S0718-28132015000100007

Vigny, C., Rudloff, A., Ruegg, J. C., Madariaga, R., Campos, J., & Alvarez, M. (2009). Upper plate deformation measured by GPS in the Coquimbo Gap, Chile. Physics of the Earth and Planetary Interiors, 175(1-2), 86-95.

Wall, R., Sellés, D. y Gana, P. (1999). Área Tiltil-Santiago, Región Metropolitana. Servicio Nacional de Geología y Minería. Mapas Geológicos N°11

Wathelet, M., 2008. An improved neighborhood algorithm: Parameter conditions and dynamic scaling. Geophys. Res. Lett. 35, 1–5. https://doi.org/10.1029/2008GL033256

Wathelet, M., 2005. Geopsy geophysical signal database for noise array processing. Software, LGIT, Grenoble.

Yañez, G., Muñoz, M., Flores-Aqueveque, V., Bosch, A., 2015. Gravity derived depth to basement in Santiago Basin, Chile: implications for its geological evolution, hydrogeology, low enthalpy geothermal, soil characterization and geo-hazards. Andean Geol. 42, 147–172.